

Intrinsically Polarized Stars and Implication for Star Formation in the Central Parsec of Our Galaxy

Tatsuhito Yoshikawa¹, Shogo Nishiyama², Motohide Tamura², Miki Ishii³
and Tetsuya Nagata¹

yosikawa@kusastro.kyoto-u.ac.jp

ABSTRACT

We have carried out adaptive-optics assisted observations at the Subaru telescope, and have found 11 intrinsically polarized sources in the central parsec of our Galaxy. They are selected from 318 point sources with $K_S < 15.5$, and their interstellar polarizations are corrected using a Stokes $Q/I - U/I$ diagram. Considering brightness, near-infrared color excess, and the amount of intrinsic polarization, two of them are good young stellar object (YSO) candidates with an age of $\sim 10^5$ yr. If they are genuine YSOs, their existence provides strong constraints on star formation mechanisms in this region. In the remaining sources, two are known as bow-shock sources in the Northern arm. One other is also located in the Northern arm and shows very similar properties, and thus likely to be a so far unknown bow-shock source. The origin of the intrinsic polarization of the other sources is as yet uncertain.

Subject headings: stars: formation — stars: pre-main sequence — Galaxy: center — polarization

1. Introduction

In the central parsec of our Galaxy, more than 100 young massive stars exist. These include helium-rich blue supergiants, Wolf-Rayet stars with ZAMS masses up to $\sim 100M_\odot$, and OB main sequence stars (Krabbe et al. 1995; Moulton et al. 2005; Paumard et al.

¹Department of Astronomy, Graduate School of Science, Kyoto University, Kyoto 606-8502

²National Astronomical Observatory of Japan, Mitaka, Tokyo 181-8588

³Subaru telescope, National Astronomical Observatory of Japan, 650 North A'ohoku Place, Hilo, HI 96720, USA

2006; Bartko et al. 2009, 2010). However, the strong tidal force from the supermassive black hole (SMBH) Sgr A* makes it very difficult for stars to be formed by gravitational collapse of a molecular cloud (Morris 1993). Investigating how the young massive stars were formed is important to understand the star formation process under the strong gravitational field from the SMBH.

Various hypotheses have been constructed to understand the presence of young massive stars near the SMBH (e.g., Alexander 2005; Genzel et al. 2010) with two of them currently favoured: the “in situ, accretion disk” scenario (e.g., Levin & Beloborodov 2003; Genzel et al. 2003) and the “inspiring star cluster” scenario (e.g., Gerhard 2001; Kim & Morris 2003). The former scenario is star formation in situ ($\lesssim 1$ pc from the SMBH) in a massive self-gravitating disk, formed by the infall of a large molecular cloud. Several numerical simulations have shown that this mechanism works well (Bonnell & Rice 2008; Hobbs & Nayakshin 2009; Alig et al. 2009). In the latter scenario, “normal” star formation occurs in a very massive star cluster tens of parsecs from the SMBH, and then the stars spiraled into the central-parsec region as a result of angular momentum loss through dynamical friction.

One method to place strong constraints on the latter scenario is to find younger stars in the central parsec, because such stars would have to be able to infall into the central parsec within their current lifetime. Recent observations using adaptive optics (AO) suggest that the young massive stars now observed were formed in a starburst 6 ± 2 Myr ago (Paumard et al. 2006; Bartko et al. 2009; Lu et al. 2013). When we assume the initial distance of a star cluster to be 30 pc from the SMBH, the required cluster mass is $\sim 10^6 M_{\odot}$ to infall to the central parsec within 6 Myr (see Equation 8 in Gerhard 2001). Although young clusters (Quintuplet and Arches) exist at the distances of ~ 30 pc (e.g., Okuda et al. 1990; Nagata et al. 1995; Figer et al. 2004), a cluster mass of $10^6 M_{\odot}$ is two-orders greater than the masses of these clusters, and as massive as the largest globular clusters. If we find stars younger than 1 Myr, such as young stellar objects (YSOs) with circumstellar disks, we can place more stringent constraints on the star formation scenario in the central parsec region.

Various papers have claimed the detection of YSO candidates in the Galactic center environment. Clénet et al. (2001) and Eckart et al. (2004) construct color-magnitude diagrams with the K and L bands to identify individual sources. Eckart et al. (2004) indicate the possibility that IRS 13N, which is a complex of extremely red sources, consists of Herbig Ae/Be objects with ages of about 0.1 to 1 Myr. Mužić et al. (2008) and Eckart et al. (2013) carry out astrometric studies of IRS 13N, and their results favor the scenario which IRS 13N is a complex of YSOs. Yusef-Zadeh et al. (2013) find 11 SiO (5-4) clumps of molecular gas within 0.6 pc of Sgr A* using ALMA (Atacama Large Millimeter/submillimeter Array) data and they interpret them as highly embedded protostellar outflows, signifying an early stage

of massive star formation in the last $10^4 - 10^5$ yr.

In this study, we use another method to detect YSOs in the Galactic center. To find YSOs with a wide range of masses, linear polarimetric observations provide effective information because many YSOs are intrinsically polarized due to the scattering of the stellar light by dust grains in their circumstellar disk. This is confirmed in model calculations (Whitney & Hartmann 1992) and observations (Tamura & Sato 1989; Tamura & Fukagawa 2005; Yudin 2000; Pereyra et al. 2009). The age of Herbig Ae/Be stars, which are intermediate mass pre-main sequence stars with circumstellar disks, are typically younger than 10^6 yr (Alonso-Albi et al. 2009) and bright enough for a detection at the distance of the Galactic center (e.g., Eiroa et al. 2002). Therefore the purpose of our study is to find Herbig Ae/Be stars in the central 1-parsec region through polarimetric observations.

Toward the central parsec, polarimetric observations are sparse; the newest one covering the entire parsec was carried out by Ott et al. (1999), whose limiting magnitude is 11 in the K band, although a much deeper observation was recently made in two strips (Buchholz et al. 2011). A few intrinsically polarized stars such as IRS 21 were reported, and they are most likely to be bow shock sources (e.g., Tanner et al. 2002, 2005, and see Section 4.2). We carried out deep polarimetric observations of the central parsec region to search for YSOs using their intrinsic polarization.

2. Observations of polarization in the central parsec

We carried out K_S -band ($2.15 \mu\text{m}$) polarimetric observations using CIAO (Coronagraph Imager with Adaptive Optics) and its polarimeter (Tamura et al. 2000, 2003) with AO36 (Takami et al. 2004) on the Subaru telescope¹ (Iye et al. 2004) on 2007 May 26 - 28. CIAO provides an image of a $22''.2 \times 22''.2$ area of the sky with a scale of $21.7 \text{ mas pix}^{-1}$. With the $R = 13.7$ mag natural guide star USNO 0600-28577051 located $\approx 20''$ from Sgr A*, and stable atmospheric conditions during the observations, AO36 provided stable correction with seeing values between $0''.15 - 0''.25$ in the K_S band through three nights.

We observed a field of $22''.2 \times 22''.2$ of the Galactic center centering Sgr A* for three nights. This corresponds to a square of $\sim 0.9 \text{ pc}$ at a distance to the Galactic center of 8 kpc (e.g., Gillessen et al. 2009). To obtain polarization, we used a rotating half-wave plate with a fixed wire grid analyzer. We made 20 sec exposures at four waveplate angles in

¹Based on data collected at Subaru Telescope, which is operated by the National Astronomical Observatory of Japan.

the sequence of 0° , 45° , 22.5° , and 67.5° (1 set) and we carried out 189 sets of observations during three nights. For checking reproducibility (see 3.1), we combined our data by each night and obtained three-one-night data sets. The integration time is 800 sec for the first night, 1140 sec for the second night, and 1500 sec for the third night; we removed 17 low-quality data sets. We processed the observed data using IRAF/DAOPHOT in a normal manner - dark subtraction, flat field correction, sky subtraction, and dead pixel correction.

3. Determination of Polarization and Selection of Intrinsically Polarized Stars

3.1. Data Analysis and Determination of Polarization

For the processed images, we carried out point spread function (PSF) photometry and aperture correction with the IRAF² tasks: *daofind*, *phot*, *psf*, and *allstar*. After combining dithered images, the area we analyzed is $17.''2 \times 17.''2$ or $0.7 \text{ pc} \times 0.7 \text{ pc}$ region. We use stars whose positions are matched within one pixel in images for four waveplate angles. Then intensities in four images for each star are used to calculate the Stokes parameters I , Q , U , the degree of polarization P , and its position angle θ using the following equations: $I = (I_0 + I_{45} + I_{22.5} + I_{67.5})/2$, $Q = I_0 - I_{45}$, $U = I_{22.5} - I_{67.5}$, $P = \sqrt{(Q/I)^2 + (U/I)^2}$, and $\theta = \frac{1}{2}\arctan(U/Q)$, where I_x is the intensity with the half wave plate oriented at x deg. The errors δP and $\delta\theta$ are calculated from the error propagation of photometric errors derived by IRAF. We normalized position angle θ by using 13 sources whose θ was determined with an accuracy of <20 deg by Ott et al. (1999). We remove the bias of P with the equation $P_{\text{db}} = \sqrt{P^2 - (\delta P)^2}$ (Wardle & Kronberg 1974), where P_{db} is the debiased degree of polarization and δP is the error of P . We calibrated the K_S -band magnitude of the stars using 61 bright ($m_{K_S} < 14$) stars in the point source catalogue by Schödel et al. (2010).

Since the AO guide star is $\simeq 20''$ far from the center of our observational field and the field of view is rather large, it can be seen in the raw image that the profile of PSF varies spatially, and in general it might be better to use a variable PSF for photometry. However, in our field, there is an insufficient number of isolated stars to reliably compute variability of the PSF and calculate an aperture correction across the field of view. We thus examine whether photometry with a variable PSF works better than a non-variable PSF by counting “good-reproducibility stars”. Here the “good-reproducibility star” is defined as a

²Image Reduction and Analysis Facility distributed by the National Optical Astronomy Observatory (NOAO), operated by the Association of Universities for Research in Astronomy, Inc. (AURA) and under cooperative agreement with the National Science Foundation (NSF).

star whose polarization has a standard deviation $\sigma_P = \sqrt{\sigma_{Q/I}^2 + \sigma_{U/I}^2}$ less than 0.01, where $\sigma_{Q/I}$ and $\sigma_{U/I}$ are calculated from the three night data sets (Figure 1). The numbers of the “good-reproducibility stars” are approximately 300 for both of the first-order-variable and non-variable PSF photometry. We therefore adopt the non-variable PSF photometry. Here the Moffat function³ is used to fit the PSFs, and after the photometry, we carried out an aperture correction. The number of the “good-reproducibility stars” with $m_{K_S} < 15.5$ is 319, and their errors are $\Delta P \approx 0.01$ (Figure 1). Through this process, we dropped $\sim 10\%$ of unsaturated, bright stars in the range of $10 < m_{K_S} < 13$.

Ott et al. (1999) observed nearly the same region as ours and obtained polarization of 41 sources. We have measured polarization for 24 out of the 41 sources; other sources observed by Ott et al. (1999) are saturated in our data, or outside our observational field. To compare these two data sets, we calculate the flux-weighted average of P and θ of the common 24 stars, resulting in $4.9\% \pm 0.2\%$ and $24^\circ \pm 1^\circ$ for our sources (statistical error only), whereas $5.1\% \pm 1.9\%$ and $34^\circ \pm 20^\circ$ for the Ott et al. (1999) data. Thus, the average degree of polarization P is consistent between the two data sets. Furthermore, although the results of Ott et al. (1999) have larger errors, our results of each star are in general consistent with theirs. For all of the 319 sources, we obtain the flux-weighted average of $P = 5.0\% \pm 0.1\%$ and $\theta = 23^\circ \pm 1^\circ$. We also obtain the average of $P = 5.2\% \pm 0.9\%$ and $\theta = 23^\circ \pm 6^\circ$, which are derived from the mean and the scatter in $Q/I - U/I$ plane (see Section 3.2). These values are consistent with the previous studies of $P = 4.1\% \pm 0.6\%$ and $\theta = 30^\circ \pm 10^\circ$ for all sources within $20'' \times 20''$ (Ott et al. 1999) and $P = 4.6\% \pm 0.6\%$ and $\theta = 26^\circ \pm 6^\circ$ for some parts of $15'' \times 15''$; (Buchholz et al. 2011). Although Buchholz et al. (2011) find higher degrees of polarization and more north-south position angles appear in the east edge of their field of view, we do not find such a tendency. To examine interstellar polarization toward the central parsec, we exclude intrinsically polarized stars ($> 3\sigma$) and calculate the flux-weighted average of P and θ . The results are $P=4.9\% \pm 0.1\%$ and $\theta = 23^\circ.6 \pm 0^\circ.2$ for 307 sources. The position angle reflects the angle of the Galactic disk (~ 31.4 deg; Reid & Brunthaler 2004).

3.2. Selecting Intrinsically Polarized Stars

To identify intrinsically polarized stars, we have to remove foreground stars first. Buchholz et al. (2009) reported 58 foreground stars from near-infrared, intermediate-band imaging with AO

³We use builtin function called “moffat15”, which is an elliptical Moffat function with a beta parameter of 1.5.

in the field of view of $\sim 40'' \times 40''$. Only two stars (their source B 275 and B 458), whose K -band extinction A_K are 1.0 and 1.9, respectively, are included in our list of the “good-reproducibility stars”. The observed color of B 275 is small ($H - K_S = 0.70$, $K_S - L' = 0.22$) and therefore it is certainly a foreground star. B 458 has similar $HK_S L'$ colors to the Galactic center sources ($H - K_S = 2.12$, $K_S - L' = 1.43$), and it is thus likely to be in the Galactic center. We treat 318 stars excluding B 275 in our analysis as stars in the central parsec. This is also confirmed from the position of $H - K_S$ and $K_S - L'$ histogram (using the H -, the K_S - and the L' -band data from Schödel et al. 2010). In Figure 2, B 275 has remarkably small values in both $H - K_S$ and $K_S - L'$. We also find that other 318 data are concentrated in the position of $H - K_S \sim 2$ and $K_S - L' \sim 1.5$. This color indicates they are sources in the central parsec (see Figure 4 in Schödel et al. 2010).

The left panel of Figure 3 is a $Q/I - U/I$ plane presentation of the polarization of all the 318 stars, and the right panel is a polarization-vector map. In the $Q/I - U/I$ plane, the vast majority of stars are concentrated in a well defined region, detached from the origin. This detachment reflects interstellar polarization, which originates from the dichroic extinction by aligned dust grains along the line of sight. The spread of the concentrated stars in the $Q/I - U/I$ diagram is estimated by fitting with Gaussian functions to remove the effect of outliers, and the standard deviations are 0.0096 in Q/I and 0.0077 in U/I (Figure 4). The spread can be attributed to both uncertainties in measurement and real variation of interstellar polarization.

Since the spread is fairly well represented by a Gaussian function, and several stars deviate by amounts not explained by the errors and the variation in interstellar polarization, we can classify these stars as intrinsically polarized stars. In selecting them, we calculated the quadratic sum σ of the polarimetric error of each star and the standard deviation of the Gaussian fitting. Here the intrinsically polarized stars are defined as stars which are apart from the peak of Q/I and U/I by $> 3\sigma$, and are listed in Table 1. The spatial distribution of them is shown in Figure 5. Figure 6 shows the intrinsic polarization vector map.

The variation in the interstellar polarization in our stars is estimated in the following way. We draw an $H - K_S$ histogram of the stars with $m_{K_S} < 15.5$ using the catalogue of Schödel et al. (2010) and fit the histogram with a Gaussian function. The resultant $H - K_S$ variation is ~ 0.23 mag. Since K-type giants are dominant with $m_{K_S} < 15.5$ in the central parsec and very little $H - K_S$ variation is expected in their intrinsic colors, we assume that the variation in $H - K_S$ is entirely due to the interstellar extinction. Concerning the relation between interstellar polarization and interstellar extinction, Hatano et al. (2013) derive the polarization efficiency toward the central 300 pc, $P_{K_S}/E(H - K_S) = 2.4\%/mag$. $E(H - K_S)$ represents color excess of $H - K_S$, and on the assumption that K-type giants are dominant

in the central parsec, we regard the variation of $H - K_S$ as that of $E(H - K_S)$. Therefore, we estimate the variation of K_S -band interstellar polarization is $\sim 0.55\%$. This value is smaller than the spread of data points in $Q/I - U/I$ diagram ($\sim 0.87\%$; Figure 3). Since the spread in $Q/I - U/I$ diagram contains the variation of interstellar polarization, our selection of intrinsically polarized stars is conservative. Toward the central parsec, there seems to be weak or no dependence of interstellar polarization on the amount of the interstellar extinction (Figure 7). Similar results are reported by Buchholz et al. (2011, see their Fig. 16). This might be related to the higher magnetic field strength of the random component compared to that of uniform component between the central parsec and us (Hatano et al. 2013).

4. Discussion

4.1. Colors of Intrinsically Polarized Stars and Their Implication for Star Formation in the Central Parsec

For YSO identification, infrared color-color diagrams are useful in assessing whether any particular star has excess emission. YSOs often exhibit infrared excesses due to thermal emission from the circumstellar disks and envelopes (e.g., Hillenbrand et al. 1992; Ishii et al. 1998; Fuente et al. 2002). Color-color diagrams can be used to distinguish between normal stellar colors that are reddened by intervening interstellar dust, and a contribution that is due to circumstellar emission. In particular, the L band is sensitive to infrared excess produced by circumstellar disks and likely the optimum wavelength for detecting infrared excesses from circumstellar disks with ground-based telescopes (Lada et al. 2000).

In Figure 8, we draw an $H - K_S$ versus $K_S - L'$ color-color diagram of intrinsically polarized stars on the basis of the infrared three-bands catalogue of the central parsec (Schödel et al. 2010). The intrinsically polarized stars are rather scattered in Figure 8, in contrast to the concentration of the majority of stars in the field along the reddening locus from main sequence and giant stars. Seven of the intrinsically polarized stars are redder than the $1-\sigma$ locus (see Figure 8), and they are shown in Figure 9 as red crosses. These seven stars probably have a circumstellar envelope which is seen nearly edge on (see Figure 9 in Robitaille et al. 2006). In particular, Stars #6 (IRS 21), #11 (IRS 2L), and #3 (IRS 10W) are even much redder than the reddest T Tauri locus. IRS 21 and IRS 10W were identified as near-infrared excess sources embedded in the minispiral and having a bow shock (Tanner et al. 2002, 2005). Viehmann et al. (2006) called them Northern Arm bow shock sources.

Additional indications of the intrinsically polarized stars may be derived from the K_S

versus $H - K_S$ color-magnitude diagram (CMD, Figure 10). The intrinsically polarized stars occupy a region of massive YSO candidates and OB stars reddened by $A_V = 30 - 50$ mag in Figure 10. In fact, the $K - L$ versus K CMD in Clénet et al. (2001) has the Northern Arm bow shock sources IRS 1W and IRS 21, which were classified as YSO candidates at that time, in the rightmost region with the reddest colors in the similar manner to Figure 10. Then in the $K - L$ versus K CMD (Clénet et al. 2001) are late-type Wolf-Rayet (WR) stars such as WC9 in the middle, and AGB stars and Ofpe/WN9 stars in the leftmost region. If some of the intrinsically polarized stars are genuine YSOs, they are very young ($\lesssim 10^{4-5}$ yr) and massive ($\gtrsim 6 - 8 M_\odot$). The presence of such young stars would indicate that these stars were formed in the central parsec, near the SMBH.

According to the “inspiraling star cluster” scenario, the required mass of a stellar cluster to infall into the central parsec from 30 pc within $\sim 10^5$ yr is $\sim 6 \times 10^7 M_\odot$ (Gerhard 2001; Gürkan & Rasio 2005), which is unreasonably massive. Even if we set the initial position of a stellar cluster to be 10 pc, the required mass is $\sim 6 \times 10^6 M_\odot$, as massive as Omega Centauri (NGC 5139). Considering the star clusters in the Galactic center (Arches, Quintuplet, and Central cluster), the typical mass of star cluster seems to be $\sim 10^4 M_\odot$ and it is not reasonable to assume $\sim 6 \times 10^6 M_\odot$. Although the circumnuclear disk (CND), which is a ringlike structure of molecular gas and dust, surrounding Sgr A* (see Figure 13 and Table 2 in Christopher et al. 2005), is the most massive and densest molecular cloud within the central 10 parsec, the total gas mass of the CND is $\sim 10^6 M_\odot$, and it is not sufficient for the formation of a star cluster like Omega Centauri. Therefore, such young stars found in the central parsec must have been formed near the SMBH and we can reject the “inspiraling star cluster” scenario if some of the intrinsically polarized stars we found are genuine YSOs. Recent studies suggest that young massive stars in the central parsec were formed in situ $\simeq 6 \pm 2$ Myr ago in a burst of star formation whose duration is less than 2 Myr (Paumard et al. 2006; Bartko et al. 2009). Since the estimated ages of the putative YSOs are significantly smaller than 6 Myr, they were possibly formed in the remnant gas of the gaseous disk. As another possibility, small-scale star formations may have been occurring intermittently in the central parsec. Christopher et al. (2005) revealed that there are 26 dense molecular gas cores in the CND. The enhanced core densities and masses may explain the formation of massive young stars.

4.2. Classification of Intrinsically Polarized Stars

Some of the intrinsically polarized stars have been spectroscopically observed (e.g., Paumard et al. 2006), and furthermore, most of them have been classified into late and early-

type stars on the basis of photometry with narrow-band filters around $2.3\ \mu\text{m}$ (Buchholz et al. 2009). Buchholz et al. (2009) classified stars in the central parsec into late- and early-type stars on the basis of characteristic CO bandhead absorption which late-type stars show in the longer wavelength part of the K band. They demonstrate that the CO bandhead depths of stars previously classified spectroscopically fall into separate regions although a few (less than 5%) early-type stars are classified as late-type and vice versa. In our sample, Star #5 could be one example of contaminations, which is classified as late-type in Buchholz et al. (2009), but it is classified as a hot “He star” using KLM two-color diagram in Viehmann et al. (2005).

Here, we classify the intrinsically polarized stars into three groups: bow shock sources in the Northern Arm (#2, #3, #4, and #6), other early-type stars (#9 and #11), and late-type stars (#1, #5, #7, #8, and #10). We discuss each group by referring to the literature.

4.2.1. Bow Shock Sources in the Northern Arm (#2, #3, #4, #6)

The Galactic center sources IRS 1W, 5, 8, 10W (Star # 6), and 21 (Star # 3) are all WR and O type stars producing bow shocks with strong winds, plowing through the ambient gas and dust of the Northern Arm, which is one stream of the minispiral (Tanner et al. 2005; Geballe et al. 2006). The positions of IRS 1W, 10W, and 21 are shown in Figure 9 as yellow circles. These sources have nearly featureless near-infrared spectra with infrared excess and often exhibit polarization that cannot be accounted for by interstellar polarization (Krabbe et al. 1995; Ott et al. 1999). Due to these features, they were first believed to be prime YSO candidates (e.g., Clénet et al. 2001). However, recent studies show that they are early-type stars whose stellar winds generate bow shocks in the Northern Arm. Therefore the infrared excess is due to re-radiation from heated dust grains and the polarization comes from scattering of the stellar light by non-spherically distributed dust (Tanner et al. 2005).

Three of the bow shock sources reported by Tanner et al. (2002, 2005) are in the current observation field of view. IRS 10W (Star #3) and IRS 21 (Star #6) exhibit intrinsic polarization in our observations. IRS 1W is not included in our list of the intrinsically polarized stars because we were able to obtain polarization of IRS 1W only during the first night due to saturation ($m_{K_S} = 9.27$ according to the first night observation). If we use the first night data, IRS 1W exhibits intrinsic polarization: $P_{\text{int}} = 8.27\%$ and $\theta_{\text{int}} = 110.9^\circ$.

In the Northern Arm, Stars #2 and #4 are also intrinsically polarized. These stars are classified as early-type stars in Buchholz et al. (2009), and Star #2 is classified as WC9 and

Star #4 is Ofpe/WN9 in Paumard et al. (2006). Star #2 might be a good YSO candidate as we mention below, but it certainly seems to be accompanied with outflow activity. Though WR stars exhibit intrinsic polarization due to scattering of free electrons in the circumstellar envelope ejected as stellar wind, the degree of polarization P is usually less than 1% (e.g., Robert et al. 1989). However, #2 and #4 show intrinsic polarizations of more than 3%. This high polarizations could be caused by the interaction between stellar wind and the minispiral, although a few WR stars do exhibit a large intrinsic polarization (3-4%, e.g., Villar-Sbaffi et al. 2006).

Star #2 is located in one of the 11 SiO (5-4) clumps of molecular gas detected by Yusef-Zadeh et al. (2013). They interpreted the SiO sources as YSO outflows, and identified a YSO candidate (source 526311) which drives the outflow, in the *SPITZER* IRAC point source catalogue (Ramírez et al. 2008). IRAC source 526311 is assigned the magnitudes of the near-infrared JHK_S ($m_J = 13.304$, $m_H = 9.439$, and $m_{K_S} = 7.898$) and the position of 2MASS. The position of Star #2 agrees with the peak of Clump 1 very well, and thus Star #2 could be the driving YSO of Clump 1.

Tanner et al. (2005) argue that the observed bow shock structures are generated by the interaction of stars rapidly moving through the Northern Arm flow, and that the bow shocks heat and perturb the dust grains associated with the Northern Arm. In this model, the intrinsic polarization angle of the source should be perpendicular to the position angle of bow shock structure (Table 3 in Tanner et al. 2005) because the position angle caused by dust scattering is perpendicular to the direction from dust to the illuminating source. The position angle of bow shock structure is calculated from the relative velocity vector of the source to the flow of the minispiral. We examine this relation in Table 2, where we calculate the position angles of bow shocks using the velocities of sources in Paumard et al. (2006) and Tanner et al. (2005) and the flow of the Northern Arm in Paumard et al. (2004).

The predicted position angles of bow shocks, however, do not necessarily agree with the direction perpendicular to the position angles of intrinsic polarization θ_{int} ; Stars #3, #4, IRS 1W are nearly perpendicular, but others are not. The discrepancy between these angles may indicate that the mechanism for generating bow shocks is not so simple. The difference was already noticed for the bow shock structure and the prediction based on the relative velocity in IRS 10W by Tanner et al. (2005). Also, note that Tanner et al. (2005) did not detect any azimuthal asymmetry in IRS 21⁴, and they interpreted this as a face-on bow shock. If this interpretation is correct and polarization is produced by scattering

⁴However, Buchholz et al. (2011) have indicated that this source is not circular in projection after applying a Lucy-Richardson deconvolution.

by surrounding dust, IRS 21 should have no large intrinsic polarization. On the contrary to this interpretation, past polarimetric studies and our observation show large intrinsic polarization. Ott et al. (1999) explain the polarization of IRS 21 by emission from hot dust aligned by the magnetic field inside the minispiral, referring to Aitken et al. (1991, 1998), who observed mid-infrared emission in the central parsec and derived the magnetic field inside the minispiral. The relation between bow shock and polarization angle is still unknown.

In these bow shock sources, Star #2 is a good YSO candidate. This star has intrinsic polarization and infrared excess, and could be the counterpart of SiO (5-4) clump. These features coincide with those of early-stage (10^{4-5} yr) YSOs.

4.2.2. Other Early-type Stars (#9, #11)

Two other intrinsically polarized stars, #9 and #11, are classified as early-type stars by Buchholz et al. (2009) and Clénet et al. (2001), respectively. Star #11 was named IRS 2L in Viehmann et al. (2006), and is one of the enigmatic sources in the central parsec. IRS 2L is one of the sources whose M -band spectra were taken and the line-of-sight absorption to IRS 2L was examined by Moulataka et al. (2009). They used the IRS 2L spectrum as a template for the foreground absorption on the assumption that IRS 2L is located close but not inside the minispiral and is not behind the circumnuclear-disk material.

IRS 2L is classified as a Be star by Clénet et al. (2001). It is known that Classical Be stars exhibit polarization due to scattering of free electrons in a circumstellar gaseous non-spherical shell (Yudin 2000). However, the degree of polarization P of classical Be stars is usually small ($0\% < P < 1.5\%$ for 95% of Be stars), and only 10 out of 495 Be stars exhibit $\sim 2\%$ (Yudin 2001). Waters & Marlborough (1992) also noted that in a framework of the single-scattering approximation and geometrically thin disks it is difficult to obtain high levels of polarization above 2%, and there is much evidence that circumstellar envelopes are optically thin (Yudin 2001). Furthermore, since self absorption of starlight in free-free and free-bound transition at their disk acts as a source of depolarization (Coyne & Kruszewski 1969), K_s -band polarization declines to $\sim 1\%$ (Pf limit ($2.28 \mu\text{m}$) is in the K_S band; see also figures of McDavid 2001). Therefore, the high intrinsic polarization of IRS 2L is not likely due to the Be star features.

Viehmann et al. (2006) studied the infrared SED of IRS 2L and find that IRS 2L has a SED of “typical luminous bow shock sources” like IRS 21 and IRS 1W. Since IRS 2L does not seem to be located inside the minispiral area (Moulataka et al. 2009), the red and featureless SED might indicate that this is a genuine YSO. We notice that other dusty sources such as

IRS 13N (Eckart et al. 2012) are still YSO candidates.

Star #9 is classified as an early-type star in Buchholz et al. (2009) and O8-9.5 III/I in Paumard et al. (2006). This star is not located in the Northern Arm, where Tanner et al. (2002, 2005) identified the dusty sources as not YSOs but as the bow shock sources, so its strong intrinsic polarization cannot be explained by the existence of a bow-shock. Thus, although Paumard et al. (2006) identified this star as a member of the clockwise rotating system whose age is $\sim 6 \pm 2$ Myr, its high degree of polarization suggests the presence of circumstellar matter, and its age might not be so certain.

In this category, we regard Star #11 as a good YSO candidate. This star, IRS 2L, has intrinsic polarization and infrared excess. If this star is not under the effect of the minispiral, this star could not be a bow-shock source but a YSO.

4.2.3. Late-type Stars (#1, #5, #7, #8, #10)

Five of the intrinsically polarized stars (#1, #5, #7, #8 and #10) are classified as late-type stars in Buchholz et al. (2009). In general, late-type stars such as red giants exhibit CO absorption, while early-type stars like OB main-sequence stars do not. However, some YSOs which are in the stage of mass accretion exhibit CO absorption (Hoffmeister et al. 2006). According to the study, CO absorption is most likely to be a sign of heavily accreting protostars with high mass accretion rates above $10^{-5} M_{\odot} \text{yr}^{-1}$. As shown in the CMD (Figure 10), our intrinsically polarized stars could be very young and be in such a heavy accretion stage. We also note that Star #5 is classified as a late-type star in Buchholz et al. (2009), but has an $L - M$ color similar to He stars, which are slightly but systematically redder than expected for hot stars (Viehmann et al. 2005). This might indicate the presence of circumstellar material. However, YSOs exhibit only weak CO absorption, if at all, and it is questionable that YSOs with weak CO absorption are classified as late-type in Buchholz et al. (2009) by narrow-band photometry. Therefore, spectroscopic studies of such a star is necessary for a firm classification.

Other possible candidates which exhibit both intrinsic polarization and CO absorption include red supergiants and post-AGB stars. Red supergiants show polarization up to several percent (e.g., Yudin 2000). However, in brightness, the five intrinsically polarized stars are unlikely to be red supergiants. In the central parsec, red supergiants are brighter than $m_K < 10.4$ (Krabbe et al. 1995). Some post-AGB stars show high polarization originating due to scattering of the stellar light by dust grains in the circumstellar envelopes, which was ejected at the final mass-loss phases (e.g., Gledhill 2005). However, Mužić et al. (2010)

calculated the expected number of post AGB star, and found less than one post AGB star in the central parsec (for more details, see 7.3 in Muzić et al. (2010)). This indicates that it is not reasonable to regard all of the five polarized stars as post AGB stars.

Thus, we cannot identify what are the five intrinsically polarized stars. Although interaction with the minispiral is possible, just like the case of the WR stars and bow shocks, most of them are not exactly in the minispiral.

5. Summary

Our high angular resolution polarimetry in the K_S band have revealed intrinsically polarized stars in the central stellar cluster. After subtraction of the interstellar polarization component, 11 intrinsically polarized stars ($> 3\sigma$) have been selected. Stars #3 (IRS 10W) and #6 (IRS 21) are bow shock sources in the Northern Arm, and Star #4 can be a similar source. These are believed to be WR stars producing bow shocks with strong winds, plowing through the ambient gas and dust, but further studies are necessary to explain the observed bow shock images and observed polarization. In the remaining eight stars, two sources (#2 and #11) are good YSO candidates because they are early type and have infrared excess. Moreover, Star #2 could be the counterpart of the SiO Clump 1, and Star #11 does not exist inside the minispiral. Observations with higher angular resolution would be of interest. Also detailed spectroscopic identifications of the other five stars thought to have CO absorption and two early-type stars is necessary.

We are grateful to R. M. Buchholz for kindly providing the narrow-band photometry data. This work was partly supported by the Grant-in-Aid for JSPS Fellows for young researchers (T.Y. and S.N.). This work was also supported by KAKENHI, Grant-in-Aid for Research Activity start-up 23840044, Grant-in-Aid for Specially Promoted Research 22000005, Grant-in-Aid for Young Scientists (A) 25707012, Grant-in-Aid Scientific Research (C) 21540240, the Global COE Program “The Next Generation of Physics, Spun from Universality and Emergence”, and Grants for Excellent Graduate Schools, from the Ministry of Education, Culture, Sports, Science and Technology (MEXT) of Japan. We especially thank the anonymous referee for constructive comments which have significantly improved the manuscript.

REFERENCES

- Aitken, D. K., Smith, C. H., Gezari, D., McCaughrean, M., & Roche, P. F. 1991, *ApJ*, 380, 419
- Aitken, D. K., Smith, C. H., Moore, T. J. T., & Roche, P. F. 1998, *MNRAS*, 299, 743
- Alexander, T. 2005, *Phys. Rep.*, 419, 65
- Alig, C., Burkert, A., Johansson, P. H., & Schartmann, M. 2009, arXiv:0908.1100
- Alonso-Albi, T., Fuente, A., Bachiller, R., Neri, R., Planesas, P., Testi, L., Berné, O., & Joblin, C. 2009, *A&A*, 497, 117
- Bartko, H., et al. 2009, *ApJ*, 697, 1741
- Bartko, H., et al. 2010, *ApJ*, 708, 834
- Bessell, M. S., & Brett, J. M. 1988, *PASP*, 100, 1134
- Bik, A., Kaper, L., & Waters, L. B. F. M. 2006, *A&A*, 455, 561
- Blum, R. D., Damineli, A., & Conti, P. S. 2001, *AJ*, 121, 3149
- Bonnell, I. A., & Rice, W. K. M. 2008, *Science*, 321, 1060
- Buchholz, R. M., Schödel, R., & Eckart, A. 2009, *A&A*, 499, 483
- Buchholz, R. M., Witzel, G., Schödel, R., et al. 2011, *A&A*, 534, A117
- Christopher, M. H., Scoville, N. Z., Stolovy, S. R., & Yun, M. S. 2005, *ApJ*, 622, 346
- Clénet, Y., Rouan, D., Gendron, E., Montri, J., Rigaut, F., Léna, P., & Lacombe, F. 2001, *A&A*, 376, 124
- Coyne, G. V., & Kruszewski, A. 1969, *AJ*, 74, 528
- Eckart, A., Genzel, R., Hofmann, R., Sams, B. J., & Tacconi-Garman, L. E. 1995, *ApJ*, 445, L23
- Eckart, A., Moulataka, J., Viehmann, T., Straubmeier, C., & Mouawad, N. 2004, *ApJ*, 602, 760
- Eckart, A., Muzic, K., Yazici, S., et al. 2012, arXiv:1208.1907
- Eckart, A., Mužić, K., Yazici, S., et al. 2013, *A&A*, 551, A18

- Eiroa, C., et al. 2002, *A&A*, 384, 1038
- Faustini, F., Molinari, S., Testi, L., & Brand, J. 2009, *A&A*, 503, 801
- Fuente, A., Martín-Pintado, J., Bachiller, R., Rodríguez-Franco, A., & Palla, F. 2002, *A&A*, 387, 977
- Figer, D. F., Rich, R. M., Kim, S. S., Morris, M., & Serabyn, E. 2004, *ApJ*, 601, 319
- Geballe, T. R., Najarro, F., Rigaut, F., & Roy, J.-R. 2006, *ApJ*, 652, 370
- Genzel, R., Pichon, C., Eckart, A., Gerhard, O. E., & Ott, T. 2000, *MNRAS*, 317, 348
- Genzel, R., et al. 2003, *ApJ*, 594, 812
- Genzel, R., Eisenhauer, F., & Gillessen, S. 2010, *Reviews of Modern Physics*, 82, 3121
- Gerhard, O. 2001, *ApJ*, 546, L39
- Gillessen, S., Eisenhauer, F., Trippe, S., et al. 2009, *ApJ*, 692, 1075
- Gledhill, T. M. 2005, *MNRAS*, 356, 883
- Gürkan, M. A., & Rasio, F. A. 2005, *ApJ*, 628, 236
- Hatano, H., Nishiyama, S., Kurita, M., et al. 2013, arXiv:1303.0456
- Hanson, M. M., Howarth, I. D., & Conti, P. S. 1997, *ApJ*, 489, 698
- Hillenbrand, L. A., Strom, S. E., Vrba, F. J., & Keene, J. 1992, *ApJ*, 397, 613
- Hobbs, A., & Nayakshin, S. 2009, *MNRAS*, 394, 191
- Hoffmeister, V. H., Chini, R., Scheyda, C. M., et al. 2006, *A&A*, 457, L29
- Ishii, M., Nagata, T., Sato, S., Watanabe, M., Yao, Y., & Jones, T. J. 1998, *AJ*, 116, 868
- Iye, M., et al. 2004, *PASJ*, 56, 381
- Jaschek, C., & Jaschek, M. 1983, *A&A*, 117, 357
- Kim, S. S., & Morris, M. 2003, *ApJ*, 597, 312
- Krabbe, A., et al. 1995, *ApJ*, 447, L95
- Lada, C. J., Muench, A. A., Haisch, K. E., Jr., et al. 2000, *AJ*, 120, 3162

- Lebofsky, M. J., Rieke, G. H., & Tokunaga, A. T. 1982, *ApJ*, 263, 736
- Leroy, J. L. 1993, *A&AS*, 101, 551
- Levin, Y., & Beloborodov, A. M. 2003, *ApJ*, 590, L33
- Li, J., An, T., Shen, Z.-Q., & Miyazaki, A. 2010, *ApJ*, 720, L56
- Lu, J. R., Do, T., Ghez, A. M., et al. 2013, *ApJ*, 764, 155
- McDavid, D. 2001, *ApJ*, 553, 1027
- Meyer, M. R., Calvet, N., & Hillenbrand, L. A. 1997, *AJ*, 114, 288
- Morris, M. 1993, *ApJ*, 408, 496
- Moultaka, J., Eckart, A., Schödel, R., Viehmann, T., & Najarro, F. 2005, *A&A*, 443, 163
- Moultaka, J., Eckart, A., & Schödel, R. 2009, *ApJ*, 703, 1635
- Mužić, K., Schödel, R., Eckart, A., Meyer, L., & Zensus, A. 2008, *A&A*, 482, 173
- Mužić, K., Eckart, A., Schödel, R., Buchholz, R., Zamaninasab, M., & Witzel, G. 2010, *A&A*, 521, A13
- Nagata, T., Woodward, C. E., Shure, M., & Kobayashi, N. 1995, *AJ*, 109, 1676
- Okuda, H., et al. 1990, *ApJ*, 351, 89
- Ott, T., Eckart, A., & Genzel, R. 1999, *ApJ*, 523, 248
- Paumard, T., Maillard, J.-P., & Morris, M. 2004, *A&A*, 426, 81
- Paumard, T., et al. 2006, *ApJ*, 643, 1011
- Pereyra, A., Girart, J. M., Magalhães, A. M., Rodrigues, C. V., & de Araújo, F. X. 2009, *A&A*, 501, 595
- Perger, M., Moultaka, J., Eckart, A., et al. 2008, *A&A*, 478, 127
- Ramírez, S. V., Arendt, R. G., Sellgren, K., et al. 2008, *ApJS*, 175, 147
- Reid, M. J., & Brunthaler, A. 2004, *ApJ*, 616, 872
- Robitaille, T. P., Whitney, B. A., Indebetouw, R., Wood, K., & Denzmore, P. 2006, *ApJS*, 167, 256

- Robert, C., Moffat, A. F. J., Bastien, P., Drissen, L., & St.-Louis, N. 1989, *ApJ*, 347, 1034
- Schödel, R., Najarro, F., Muzic, K., & Eckart, A. 2010, *A&A*, 511, A18
- Takami, H., et al. 2004, *Proc. SPIE*, 5490, 837
- Tamura, M., & Sato, S. 1989, *AJ*, 98, 1368
- Tamura, M., et al. 2000, *Proc. SPIE*, 4008, 1153
- Tamura, M., Fukagawa, M., Murakawa, K., et al. 2003, *Proc. SPIE*, 4843, 190
- Tamura, M., & Fukagawa, M. 2005, *Astronomical Polarimetry: Current Status and Future Directions*, 343, 215
- Tanner, A., Ghez, A. M., Morris, M., Becklin, E. E., Cotera, A., Ressler, M., Werner, M., & Wizinowich, P. 2002, *ApJ*, 575, 860
- Tanner, A., Ghez, A. M., Morris, M. R., & Christou, J. C. 2005, *ApJ*, 624, 742
- Viehmann, T., Eckart, A., Schödel, R., Moulataka, J., Straubmeier, C., & Pott, J.-U. 2005, *A&A*, 433, 117
- Viehmann, T., Eckart, A., Schödel, R., Pott, J.-U., & Moulataka, J. 2006, *ApJ*, 642, 861
- Villar-Sbaffi, A., St-Louis, N., Moffat, A. F. J., & Piirola, V. 2006, *ApJ*, 640, 995
- Wardle, J. F. C., & Kronberg, P. P. 1974, *ApJ*, 194, 249
- Wainscoat, R. J., Cohen, M., Volk, K., Walker, H. J., & Schwartz, D. E. 1992, *ApJS*, 83, 111
- Waters, L. B. F. M., & Marlborough, J. M. 1992, *A&A*, 256,195
- Whitney, B. A., & Hartmann, L. 1992, *ApJ*, 395, 529
- Yudin, R. V. 2000, *A&AS*, 144, 285
- Yudin, R. V. 2001, *A&A*, 368, 912
- Yusef-Zadeh, F., Royster, M., Wardle, M., et al. 2013, *ApJ*, 767, L32

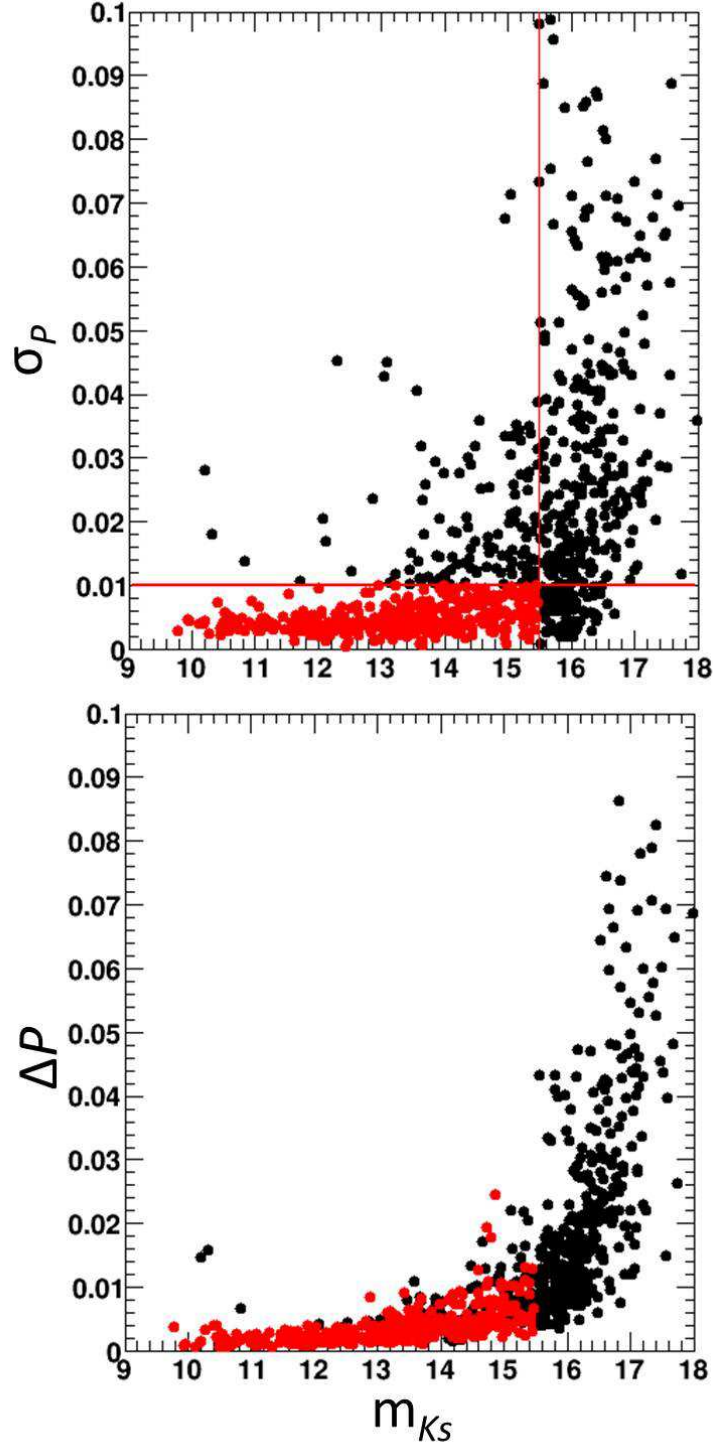


Fig. 1.— Scatterplots of σ_P vs. m_{K_S} (*top*) and ΔP vs. m_{K_S} (*bottom*), where σ_P represents the standard deviation of polarization of each object during three nights (see text) and ΔP is polarimetric error obtained by IRAF/DAOPHOT photometry. Stars with $\sigma_P < 0.01$ and $m_{K_S} < 15.5$ are defined as “good-reproducibility stars” (red plot), and used in our analysis.

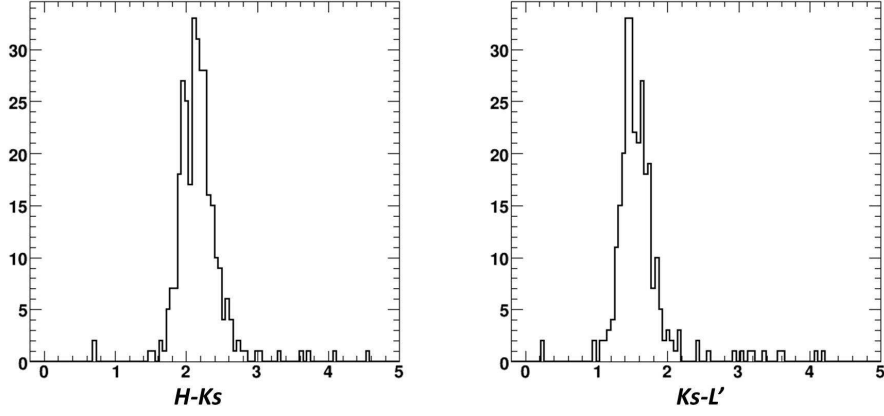


Fig. 2.— Histograms of $H - K_S$ (*left*) and $K_S - L'$ (*right*) for “good-reproducibility stars”, for which we use the H - and L' -band data from Schödel et al. (2010).

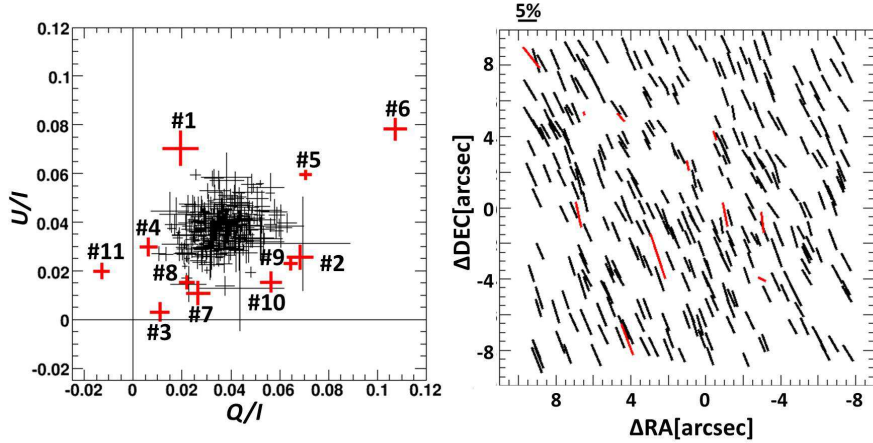


Fig. 3.— *left*: A $Q/I - U/I$ plane - a scatterplot of U/I vs. Q/I for “good-reproducibility stars”, excluding a foreground star (B 275). The colors of data points represent the significance of intrinsic polarization of sources. Black cross represents $< 3\sigma$ and red cross is $> 3\sigma$. Here, σ is the rms of photometric error and spread of data points. Number in this figure (#1, #2, and so on) corresponds to the column 1 in Table 1. *right*: A polarization vector map for “good-reproducibility stars”, excluding the foreground star. The length and the angle of bars represent P and θ , respectively. The colors of bars have the same meaning as left figure.

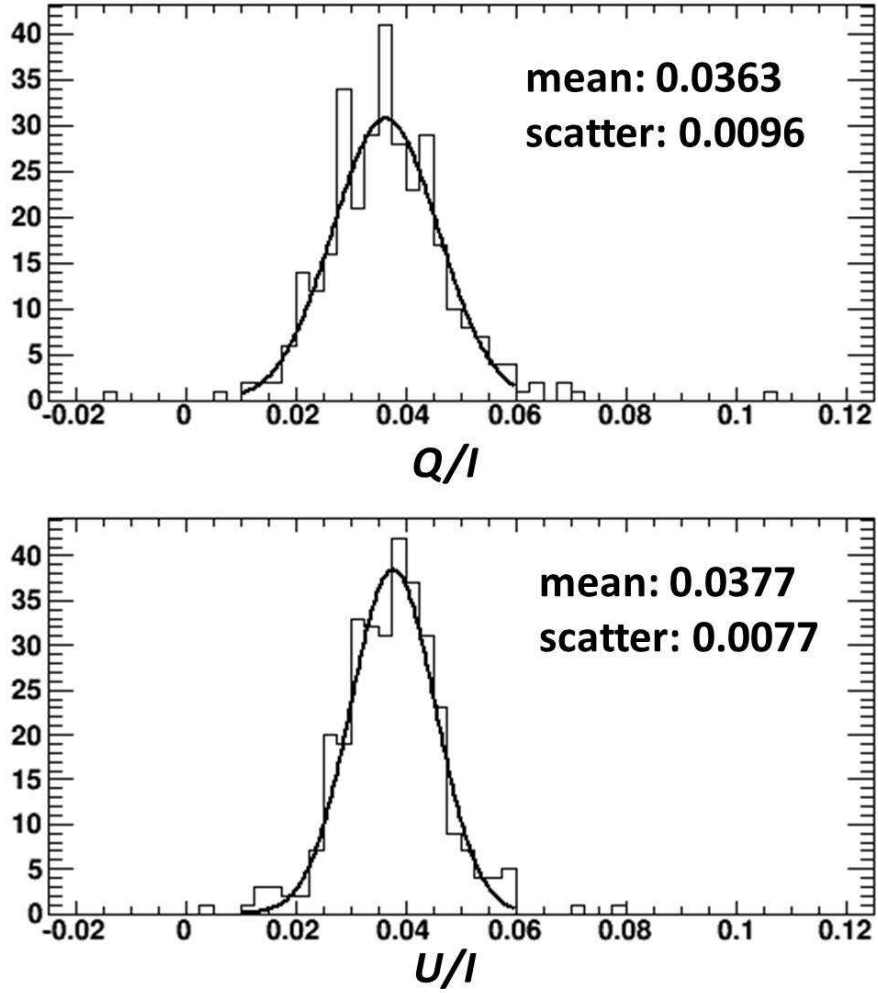


Fig. 4.— Histograms of Q/I (*top*) and U/I (*bottom*) for “good-reproducibility stars”, excluding a foreground star. Black solid curves are fitted with Gaussian functions.

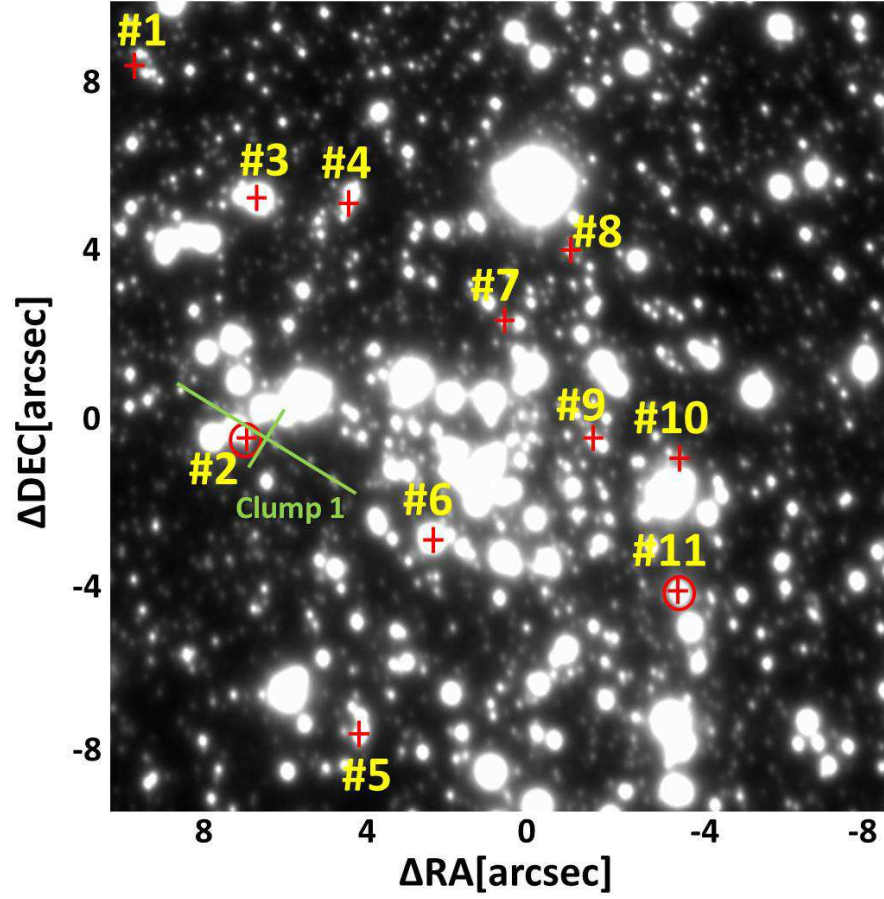


Fig. 5.— The spatial distribution of intrinsically polarized stars. Red cross represents a $> 3\sigma$ polarized object and circled ones (#2 and #11) are good YSO candidates (see Discussion). Green cross represents the position of SiO (5-4) Clump 1, and the length of cross corresponds to the spatial resolution of $2''.61 \times 0''.97$ (Yusef-Zadeh et al. 2013).

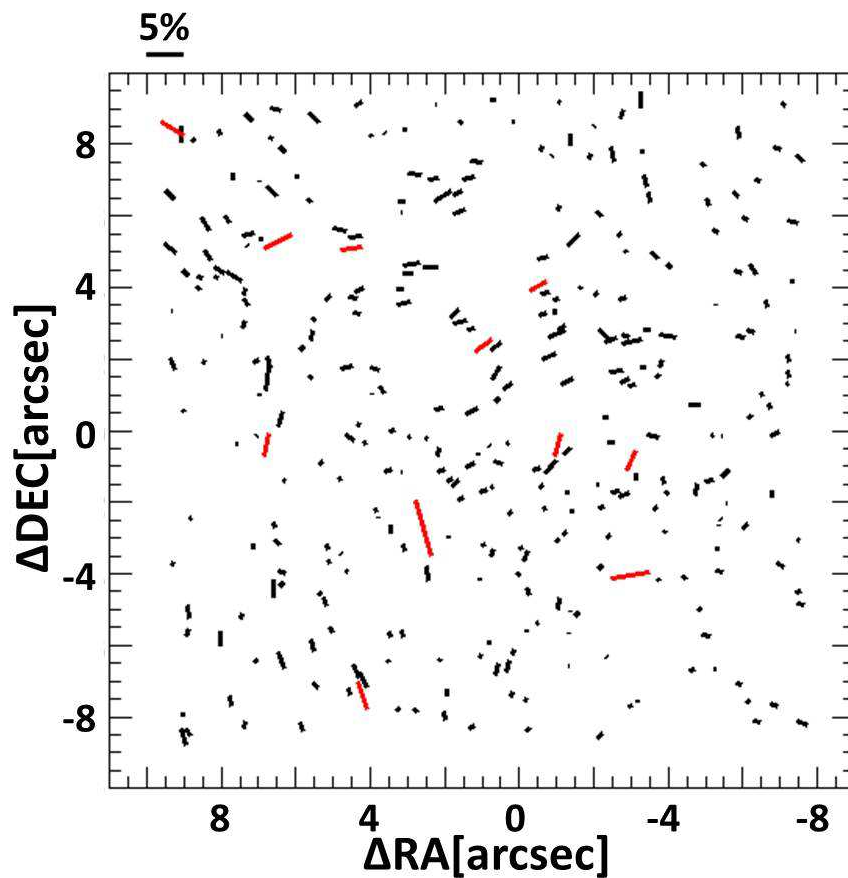


Fig. 6.— Intrinsic polarization vector map. We calculate intrinsic polarization by subtracting the average of interstellar polarization in this field $(Q_{\text{peak}}, U_{\text{peak}}) = (0.0363, 0.0377)$ from Stokes parameters (Q, U) of each star. Red and black lines represent stars whose intrinsic polarization is detected as more than 3σ and less than 3σ , respectively.

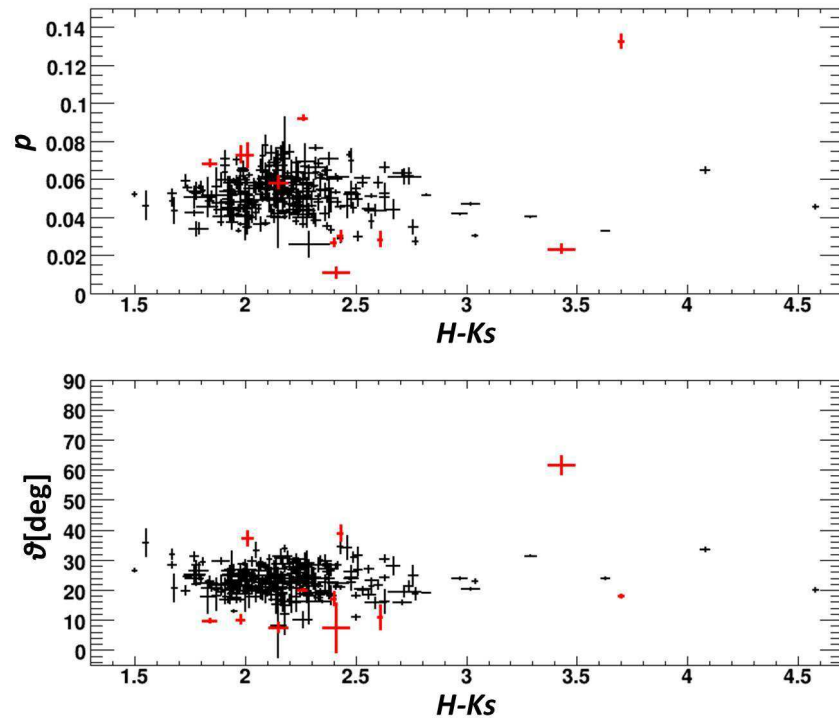


Fig. 7.— Scatterplots of P vs. $H - K_S$ (*top*) and θ vs. $H - K_S$ (*bottom*). Red plot is a $> 3\sigma$ polarized object.

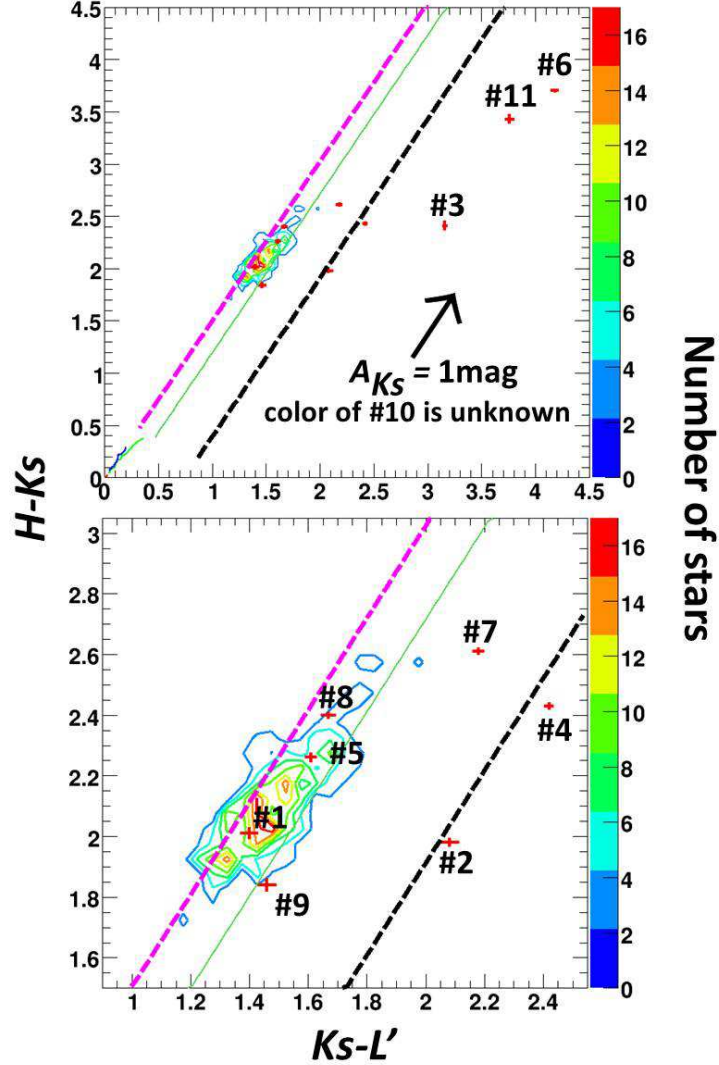


Fig. 8.— $HK_S L'$ color-color diagram. The contour is drawn with stars in the field of our observations, whose K_S -band magnitudes are less than 15.5 mag and L' -band magnitudes are obtained in (Schödel et al. 2010). The red cross represents a $> 3\sigma$ polarized object. Two dashed lines represent the extended loci along reddening vector (Schödel et al. 2010). The magenta dashed line is for OBA-type main sequence + GKM-type giant (Bessell & Brett 1988) and the black dashed line is for T Tauri stars (Meyer et al. 1997). Solid lines in the lower left corner of this figure represent the colors of OBA dwarfs (red), FGKM dwarfs (green), GKM giants (blue), OBA supergiants (yellow) and FGKM supergiants (magenta), respectively (Bessell & Brett 1988). The contour of color of all stars in the observational field are superposed and green thin solid line is 1σ of dispersion when we fit the histogram of color of stars with a Gaussian function along the vertical direction to reddening vector. Lower panel is zoom-in view. Note that one 3σ source is not plotted because the L' -band magnitude is not in the catalogue of (Schödel et al. 2010).

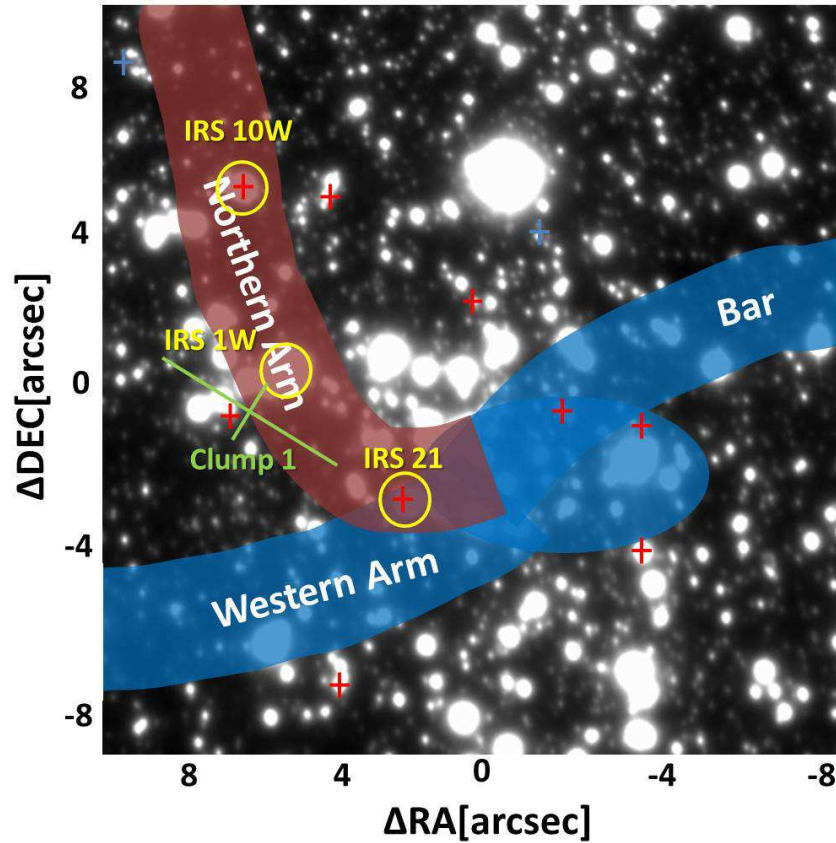


Fig. 9.— The schematic view of the minispiral is superimposed on the K_S -band image and the spatial distribution of intrinsically polarized stars. Red cross has infrared excess in Figure 8, and blue cross does not. Green cross represents the position of SiO (5-4) Clump 1, and the length of cross corresponds to the spatial resolution of $2''.61 \times 0''.97$ (Yusef-Zadeh et al. 2013). Bow shock sources along the Northern Arm studied by Tanner et al. (2002, 2005) are indicated by yellow circles.

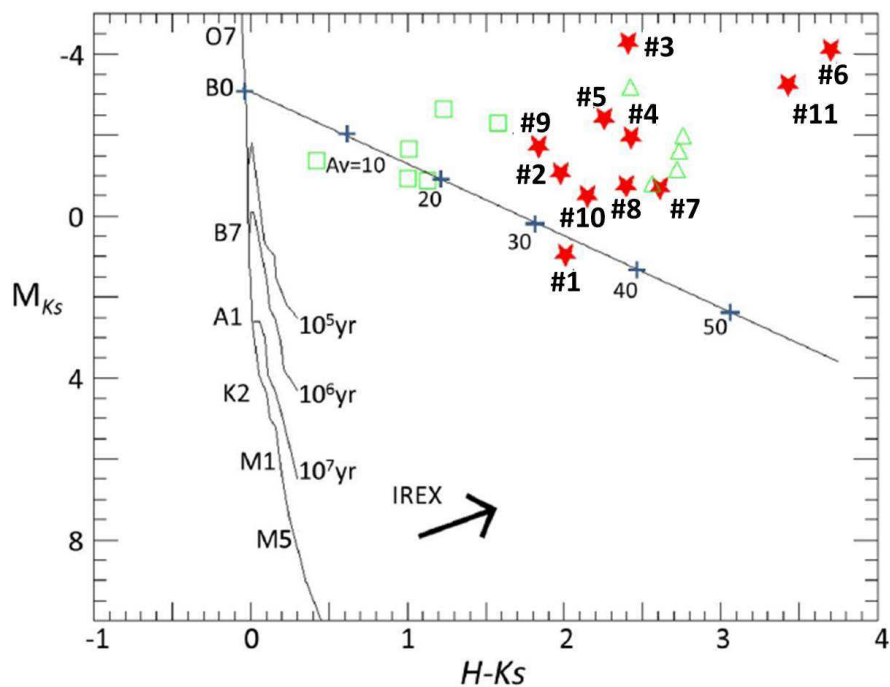


Fig. 10.— Color-magnitude diagram (M_{K_s} vs. $H - K_s$) of our YSO candidates and other massive YSO candidates. Superposed are the main sequence (leftmost curve), reddening line (diagonal line), isochrones for pre-main sequence stars (four full lines) and, infrared-excess arrow (Figure 5 in Faustini et al. 2009, and references therein). Filled star marks represent our YSO candidates and the numbers corresponds to the numbers in 1. Green symbols represent massive YSO candidates from other studies: squares are from Hanson et al. (1997) and triangles are from Blum et al. (2001).

Table 1: The features of intrinsically polarized stars ($> 3\sigma$).

ID	ΔRA^a (arcsec)	ΔDEC^a (arcsec)	m_{K_s} (mag)	$(Q/I, U/I)$	$p_{\text{int}}, \theta_{\text{int}}^b$ (%, deg)	$(H - K_s, K_s - L')$ (mag)	identification/ classification
1	9.59	8.56	15.48	(0.020, 0.070)	(3.6±0.7, 59±5)	(2.01, 1.40)	late ^d
2	6.91	-0.38	13.48	(0.069, 0.026)	(3.4±0.5, 170±4)	(1.98, 2.08)	WC9? ^c , early ^d
3 ^h	6.60	5.38	10.26	(0.011, 0.003)	(4.3±0.3, 117±2)	(2.41, 3.16)	IRS 10W ^e
4	4.49	5.17	12.60	(0.006, 0.030)	(3.1±0.3, 97±3)	(2.43, 2.42)	Ofpe/WN9, IRS 7E2 ^c
5	4.17	-7.49	12.12	(0.071, 0.059)	(4.1±0.2, 16±1)	(2.26, 1.61)	late ^d , He star ^f
6 ^h	2.43	-2.76	10.42	(0.107, 0.078)	(8.2±0.4, 15±1)	(3.70, 4.18)	IRS 21 ^e
7	0.74	2.41	13.83	(0.027, 0.011)	(2.8±0.4, 125±4)	(2.61, 2.18)	late ^d
8	-0.83	4.11	13.80	(0.022, 0.015)	(2.7±0.2, 119±3)	(2.40, 1.67)	late ^d
9	-1.40	-0.38	12.81	(0.065, 0.023)	(3.2±0.2, 166±2)	(1.84, 1.46)	O8-9.5 III/I, W10 ^c , early ^d
10	-3.51	-0.80	14.05	(0.057, 0.015)	(3.0±0.4, 156±4)	(2.15, -)	late ^d
11	-3.49	-4.06	11.29	(-0.013, 0.020)	(5.2±0.3, 100±2)	(3.43, 3.76)	IRS 2L ^e , Be star ^g

^a The origin is Sgr A* (RA = 17:45:40.04, DEC = -29:00:28.17).

^b Values of this column are calculated by subtracting $(Q/I_{\text{peak}}, U/I_{\text{peak}}) = (0.0363, 0.0377)$ from observed $(Q/I, U/I)$.

^c Spectral type and object name from Paumard et al. (2006).

^d Late/early type from Buchholz et al. (2009).

^e Object name from Viehmann et al. (2005).

^f Based on *KLM* two-color diagram in Viehmann et al. (2005).

^g Based on $K - L$ versus K CMD in Clénet et al. (2001).

^h Known bow-shock sources in Tanner et al. (2002, 2005).

Table 2: Calculated position angles of bow shock and polarization angles.

ID	PA _{bowshock} ^a	PA _{polarization} ^b
2	20	170
3 (IRS 10W)	10	120
4	30	100
6 (IRS 21)	-20	15
IRS 1W ^c	5	110

^a PA_{bowshock} corresponds to the direction of relative velocity vector between the DES and the Northern Arm flow on the plane of the sky.

^b PA_{polarization} corresponds to θ_{int} in Table 1.

^c IRS 1W is measured in only the first day in our observations.

NOTE.-We cannot obtain position angles of #9 and #11 because they exist inside the bar, which is one stream of the minispiral and Paumard et al. (2004) have only the data of the Northern Arm.